Stabilizing Josephson radiation in the presence of thermal noise

bachelor's thesis

Submitted to the Faculty of Mathematics, Computer Science and Natural Sciences at RWTH Aachen University

presented by

Jonas Völler

under the supervision of

Prof. Dr. Fabian Hassler

and

Prof. Dr. Markus Müller

JARA-Institute for Quantum Information

11/2023

Abstract

This thesis investigates the stability of Josephson radiation emitted in a thermalized environment. We introduce the AC Josephson effect as a radiation source and implement it in a circuit that has the properties of a clock consisting of an oscillator and a continuous counter. The correlation of the emitted light is characterized by the first-order coherence, for which we obtain explicit analytical expressions. We discuss the limited coherence properties of the simple Josephson circuit and explain how this result can be improved by using the clock circuit. For the latter, our calculations reveal a parameter that allows us to enhance its stability.

Contents

Chapter 1

Introduction

The Josephson radiation is an electromagnetic signal that is emitted when a junction between two superconductors is voltage-biased [1]. An experimental measurement of such radiation serves as a demonstration of the AC Josephson effect. The pursuit of new stable radiation sources holds inherent value, as applications of lasers can be found in numerous scientific and everyday fields, including medical and computer-based sectors. However, the coherence properties of the Josephson radiation are limited by the environment surrounding the junction. This includes electromagnetic effects and the thermal state of the system. Recent advancements have made it possible to achieve the regime of Josephson lasing by tailoring the environment from which the radiation is emitted [2].

In this thesis, we are interested in the thermal aspect that prohibits Josephson radiation from having long coherence times, which is essential for the realisation of a laser. To that end, in Ch. 2, the AC Josephson effect is introduced first with an ideal and then with a realistic voltage source. For the latter, we use the Resistively and Capacitively Shunted Junction model and discuss under which assumptions it can be considered in the classical regime. We then modify the simple Josephson circuit by adding another branch consisting of a second Josephson junction in series with an RLC circuit, obtaining a circuit with characteristics similar to a traditional clock. Remaining in the classical regime, we derive the equation of motion for the current in the circuit and, from there, find an analytical description of the superconducting phases at different nodes using the rotating wave approximation.

The mathematical description of a thermal environment is given by the Johnson-Nyquist noise, which is introduced in Ch. 3. We focus on the low-temperature

regime and show how thermal noise acts on circuits including Josephson junctions. The coherence of the emitted radiation is quantified by the use of the first-order coherence. We obtain an analytical expression for the correlation functions of both the Josephson and the clock circuit and discuss the results. Throughout the entire thesis, numerical simulations are used to back up the analytical calculations.

Chapter 2

Sources of Josephson radiation

2.1 The ideal AC Josephson effect

The Josephson junction is an electrical component that B.D. Josephson first analysed in 1962 [3]. It consists of two superconductors separated by an insulating barrier. If the thickness of the insulator is small enough, the quantum mechanical amplitude of the electrons enables tunnelling through the barrier. As explained in [4], if there is no magnetic field, the Schrödinger equation for such a system is given by

$$i\hbar\frac{\partial}{\partial t}\begin{pmatrix}\psi_1\\ \psi_2\end{pmatrix} = \begin{pmatrix}\frac{qV}{2} & K\\ K & -\frac{qV}{2}\end{pmatrix}\begin{pmatrix}\psi_1\\ \psi_2\end{pmatrix}, \tag{2.1}$$

with Planck's constant $\hbar$ and the wave functions $\psi_{1/2} = \sqrt{\rho_{1/2}}e^{i\theta_{1/2}}$, where $\rho_{1/2}$ are the electron densities and $\theta_{1/2}$ the phases on either side of the junction. Here, the squares of the wave functions $|\psi_{1/2}|^2$ denote the probabilities of finding an electron on the insulator's left or right-hand side, respectively. Furthermore, V is a DC voltage being applied to the system, creating a potential difference between the superconductors and q is the charge of an electron pair $q = 2e$. The final parameter, K, is a characteristical constant of the junction that quantifies the coupling. Were K zero, the matrix would be diagonal, and the two differential equations would decouple, leaving us with the ground states of both superconductors. Instead, $K \neq 0$ allows currents to flow through the junction. The entire setup is depicted in Fig. 2.1.

Now we can define φ as the phase-difference $\varphi = (\theta_1 - \theta_2)$ and sort for the real

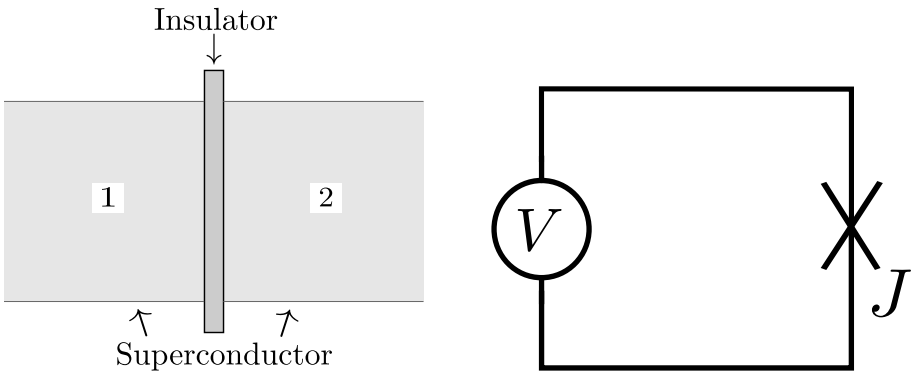

Figure 2.1: (a) Schematic depiction of a Josephson junction with two superconductors and an insulating barrier in between [4]. (b) Ideal Josephson circuit with a Josephson junction J and a DC voltage V.

and imaginary parts in Eq. (2.1), which leads to four new equations [4]

$$\begin{aligned}
\dot{\rho}_1 &= \frac{2}{\hbar} K \sqrt{\rho_1 \rho_2} \sin(\varphi) \\
\dot{\rho}_2 &= -\frac{2}{\hbar} K \sqrt{\rho_1 \rho_2} \sin(\varphi) \\
\dot{\theta}_1 &= -\frac{K}{\hbar} \sqrt{\frac{\rho_2}{\rho_1}} \cos(\varphi) - \frac{qV}{2\hbar} \\
\dot{\theta}_2 &= -\frac{K}{\hbar} \sqrt{\frac{\rho_1}{\rho_2}} \cos(\varphi) + \frac{qV}{2\hbar}
\end{aligned} \tag{2.2}$$

that fully define the wave functions. With $\dot{\rho}_1 = -\dot{\rho}_2$ and finite coupling, there is a current flowing from the first into the second region, which is negated by additional currents flowing due to the applied voltage[1]. In total, this keeps the electron densities constant over time. Starting from equilibrium, we thus have $\rho_1 = \rho_2 = \rho_0$. Solving the four equations then yields the two Josephson equations

$$I(t) = I_c \sin(\varphi(t)) \tag{2.3a}$$

$$\frac{\partial \varphi}{\partial t} = \frac{2eV}{\hbar}, \tag{2.3b}$$

where the critical current $I_c = \frac{2K\rho_0}{\hbar}$ is again a characteristical constant of the junction. By integrating the phase change $\dot{\varphi}$ for a constant voltage and inserting it into the first Josephson equation, we observe that the superconducting

[1] If there were no extra electric forces, $\dot{\rho}_1 = -\dot{\rho}_2$ would express a charging of the second region. This does not happen because the potential is constant, and there are currents flowing to prevent this from changing.

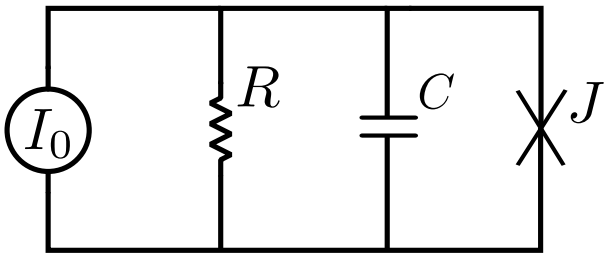

Figure 2.2: Realistic Josephson circuit according to the RCSJ model. It includes a voltage source, which is made up of a DC current source and a resistor, as well as a capacitor and the junction itself.

phase varies linearly over time, which leads to an AC current flowing out of the junction with the amplitude I_c and the frequency $\omega_0 = \frac{2eV}{\hbar}$

$$\varphi(t) = \frac{2e}{\hbar} Vt \Rightarrow I(t) = I_c \sin(\omega_0 t). \tag{2.4}$$

Here, we integrate from $t_0 = 0$ and insert $\varphi(0) = 0$.

2.2 AC Josephson effect with real voltage sources

In reality, creating an ideal voltage source is impossible, as it would require zero internal resistance. A more realistic description of a Josephson junction with a real voltage source is given by the **Resistively and Capacitively Shunted Junction model**, in short, the RCSJ model [5]. It consists of a DC current source I_0, a voltage-independent resistor R, a capacitor C and the Josephson junction itself, as shown in Fig. 2.2. Under the assumption that the resistance is small $R \ll R_Q = h/4e = 6.45k\Omega$, the classical regime is recovered because the quantum fluctuations of the charge operator $\hat{Q}$ are suppressed far below $2e$, the charge of a Cooper pair [6]. From the conservation of the supplied current, we can then derive the following equation of motion

$$I_0 = I_c \sin(\varphi) + C\frac{dV}{dt} + \frac{V}{R}, \tag{2.5}$$

where we only considered the low temperature limit, omitting noise terms, which we will be taking into account in Ch. 3.

The mean current flowing through an AC voltage biased capacitor is given by $I = C\omega V$, with ω the frequency of the voltage. The same voltage leads to a current $I = \frac{V}{R}$ in a resistor. Together with the plasma frequency of the junction [7] $\omega_p = \sqrt{\frac{2eI_c}{\hbar C}}$, we find that for an overdamped circuit with $R \ll \frac{1}{\sqrt{2eI_cC/\hbar}}$, the contribution of the capacitance in the RCSJ model can be neglected, yielding

$$I_0 = I_c \sin(\varphi) + \frac{1}{\tilde{R}}\dot{\varphi}, \tag{2.6}$$

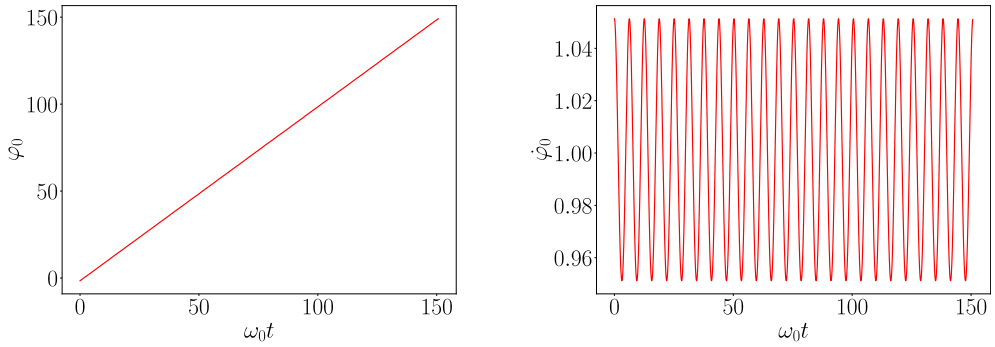

(a) (b)

Figure 2.3: Graphical depiction of φ_0 and $\dot{\varphi}_0$ with $I_0 = 1A$, $I_c = 0.05A$ and $\omega_0 = 1Hz$.(a) Linear trajectory of the superconducting phase $\varphi_0(t)$. (b) Trajectory of the phase change $\dot{\varphi}_0(t)$, oscillating around a constant value.

where we insert the second Josephson equation and summarise $\tilde{R} = \frac{2e}{\hbar}R$. We can now make a distinction between two cases. In the first case, $I_0 < I_c$, the driving current is too small for the electrons to overcome the potential barrier, resulting in no currents flowing. Instead, assuming the driving current to be large compared to the critical current of the junction, meaning $I_0 \gg I_c$, lets us integrate over φ and t and find an expression for the superconducting phase[2]

$$\begin{aligned} \frac{1}{\tilde{R}} \int_{-\frac{\pi}{2}}^{\varphi_0} \frac{d\varphi}{I_0 - I_c \sin(\varphi)} &= \int_{t_0}^{t} dt' \\ \Rightarrow \quad \varphi_0(t) &= 2 \arctan\left(\frac{I_0 + I_c}{\sqrt{I_0^2 - I_c^2}} \tan\left(\frac{\pi}{T}(t - t_0) \right) \right) - \frac{\pi}{2}. \end{aligned} \tag{2.7}$$

with the period $T = \frac{2\pi}{\tilde{R}\sqrt{I_0^2 - I_c^2}}$, which we get from integrating over φ from 0 to 2π. The phase change can then be calculated by taking the derivative with respect to the time

$$\dot{\varphi}_0(t) = \omega_0 \frac{\sqrt{I_0^2 - I_c^2}}{I_0 - I_c \cos(\omega_0(t - t_0))}, \tag{2.8}$$

with the frequency $\omega_0 = \frac{2\pi}{T}$. Thus, the voltage arising from the varying phase change is given by

$$V(t) = R \frac{I_0^2 - I_c^2}{I_0 - I_c \cos(\omega_0(t - t_0))}. \tag{2.9}$$

In Fig. 2.3, it is shown that the superconducting phase follows a linear trajectory, as it did with the ideal voltage source. Moreover, the phase change, which

[2]Starting at $-\pi/2$ simplifies the integration of φ and causes the oscillation of the phase change to start with a maximum.

defines the outgoing current, oscillates around a constant component.

2.3 Clock circuit using the AC Josephson effect

After discussing the AC Josephson effect as a possible radiation source, we can now utilise it to build a clock-like circuit. As proposed in [8], two components are needed to build a clock. The first one is an oscillating degree of freedom, X, which is then coupled to the second component, a counting degree of freedom, Y. The coupling has to work so that X forces its oscillation onto Y, synchronising both components while simultaneously Y provides X with enough energy to sustain a constant oscillation. Mathematically, this can be described as a system of differential equations of the form

$$\gamma\dot{X} + \ddot{X} + \omega^2 X = \kappa \sin(Y) \tag{2.10a}$$

$$\Gamma\dot{Y} = f + \kappa X \cos(Y), \tag{2.10b}$$

where ω is the frequency of the oscillator and κ is the parameter controlling the coupling of the subsystems. Furthermore, f describes a constant driving force, analogous to the case of a grandfather clock, where the gravity exerts a force on the weights driving the pendulum. The final two parameters, γ and Γ, are damping constants. We will focus on the case of an underdamped harmonic oscillator, corresponding to $\gamma \ll 1$, and an overdamped counter, such that all degrees of freedom can be calculated classically.

It is possible to find a circuit that utilises the AC Josephson effect and, under the right conditions, implements Eq. (2.10). For this, we extend the simple Josephson circuit by a second branch consisting of a damped harmonic oscillator in the form of an RLC circuit in series with a Josephson junction, as shown in Fig. 2.4. Using Kirchhoff's current law at the nodes of X and Y yields

$$I_{cb}\sin(Y - X) = C\frac{\hbar}{2e}\ddot{X} + \frac{1}{L}\frac{\hbar}{2e}X + \frac{1}{R_{LC}}\frac{\hbar}{2e}\dot{X} \tag{2.11a}$$

$$I_0 = \frac{1}{R}\frac{\hbar}{2e}\dot{Y} + I_{ca}\sin(Y + c) + I_{cb}\sin(Y - X). \tag{2.11b}$$

The observables X and Y are now defined as the superconducting phases at the depicted nodes, where, similar to the simple Josephson circuit, we assume the inert capacitances of J_a and J_b to be negligible compared to the conductances, thus describing the current flowing out of the junctions by $I = I_c \sin(\varphi)$. c is an additional phase coming from the external magnetic flux through the

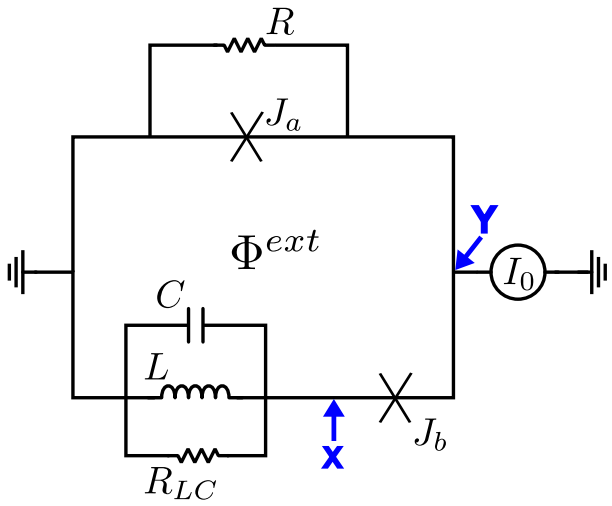

Figure 2.4: Circuit consisting of an upper branch with a Josephson junction J_a and a small resistor R as well as a lower branch consisting of an RLC circuit and another Josephson junction J_b. The circuit is powered by a DC current source I_0 and has an external magnetic flux Φ^{ext} passing through it. Lastly, the nodes at which we define the variables X and Y are shown in blue.

circuit Φ^{ext}, that can be tuned to give $c = \pi$. Furthermore, we choose the critical currents of both junctions to be equal $I_{ca} = I_{cb} = I_c$. Introducing the parameters

$$\kappa = \frac{2eZ_0I_c}{\hbar}\omega,\ f = \kappa\frac{I_0}{I_c},\ \gamma = \frac{Z_0}{R_{LC}}\omega,\ \Gamma = \frac{Z_0}{R}\omega,$$

with the impedance $Z_0 = \sqrt{\frac{L}{C}}$ and the natural frequency of the RLC circuit $\omega = \sqrt{\frac{1}{LC}}$, we obtain a simplified version of Eq. (2.11)

$$\kappa\sin(Y - X) = \ddot{X} + \omega^2 X + \gamma\dot{X} \tag{2.12a}$$

$$f = \Gamma\dot{Y} - \kappa\sin(Y) + \kappa\sin(Y - X). \tag{2.12b}$$

These equations correspond to Eq. (2.10) in the regime of small oscillation amplitudes $X \ll 1$, such that X is sufficiently small to allow for taylor expanding the $\sin(Y - X)$ terms.

Without the coupling term, Eq. (2.10b) describes a massless particle moving at constant velocity, where the solution is known from classical mechanics as $Y = \frac{f}{\Gamma}t + \theta = \omega' t + \theta$. Revisiting the idea of a clock, Y then continuously counts the time with the speed $\omega' = \frac{f}{\Gamma}$. As for the oscillating degree of freedom X, it has to maintain a stable amplitude $A \in \mathbb{R}$ and frequency ω in order to satisfy the requirements of a clock. We can express this as $X = \mathrm{Re}\left(Ae^{i(\omega t+\varphi)}\right)$. Circling

back to the case with non-zero coupling, the frequencies of both variables have to align $\omega_X = \omega_Y$ in order to create a synchronisation. A sensible ansatz is therefore given by

$$\begin{aligned} X(t) &= \mathrm{Re}\left(Ae^{-i(\omega t+\varphi(t))}\right) \\ Y(t) &= \omega' t + \theta(t), \end{aligned} \tag{2.13}$$

with the phases $\varphi(t) = \dot{\varphi}t + \varphi_0$ and $\theta(t) = \dot{\theta}t + \theta_0$ both being slow variables, meaning $\varphi(t)$ and $\theta(t)$ change over much larger time scales than ω^{-1} and ω'^{-1}. This is equivalent to the assumption that $\dot{\varphi} \ll \omega$, and $\dot{\theta} \ll \omega'$. From the synchronisation, we get the equation

$$\omega_X = \omega_Y \Leftrightarrow \omega + \dot{\varphi} = \omega' + \dot{\theta}, \tag{2.14}$$

leaving $\dot{\varphi}$ and $\dot{\theta}$ to be determined. We can calculate them by revisiting the starting point (Eq. (2.10)) and inserting the analytical ansatz. For the first equation, we now use the complex form of X, before taking the real part. Omitting small terms of $\mathcal{O}\left(\dot{\varphi}^2\right)$ as well as $\mathcal{O}\left(\gamma\dot{\varphi}\right)$ and sorting for real and imaginary parts yields

$$\begin{aligned} \dot{\varphi} &= \frac{\kappa}{2A\omega}\sin(\varphi_0 - \theta_0) \\ \frac{A\omega}{\kappa}\gamma &= -\cos(\varphi_0 - \theta_0). \end{aligned} \tag{2.15}$$

For Eq. (2.10b), we use the trigonometric addition theorems to expand the equation into a slow and a fast oscillation. Now the slow oscillation loses its time dependency and gives a constant contribution. Making a **Rotating wave approximation**, in short RWA, the antiresonant fast oscillation can be dropped by averaging it over one or multiple periods [9], leaving only the constant term

$$\begin{aligned} \dot{\theta} &= \frac{\kappa A}{\Gamma}\cos(\omega t + \varphi)\cos(\omega' t + \theta) \\ &= \frac{\kappa A}{2\Gamma}\left[\cos((\omega - \omega')t + \varphi - \theta\right) + \cos((\omega + \omega')t + \varphi + \theta)] \\ &\approx \frac{\kappa A}{2\Gamma}\cos(\varphi_0 - \theta_0). \end{aligned} \tag{2.16}$$

We thus found a set of equations, that describes the time derivatives of the phases and the amplitude of the oscillation, while only depending on our fixed parameters and the constant phase difference $(\varphi_0 - \theta_0)$

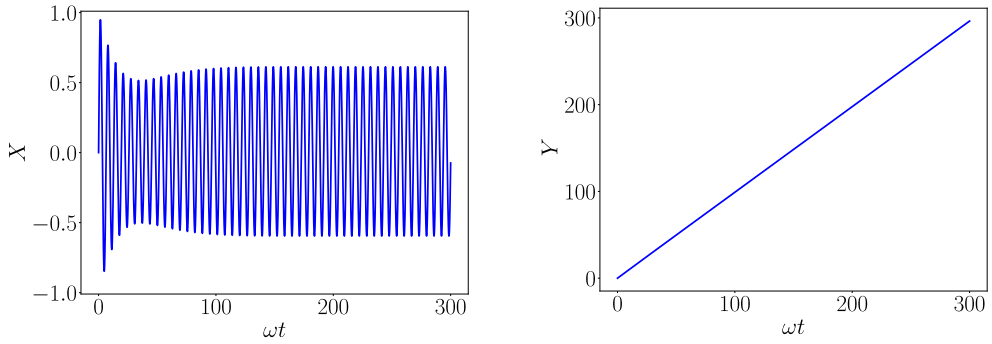

(a) (b)

Figure 2.5: Numerical simulation of Eq. (2.10) with $\delta = 0.001$, $\kappa = 0.05$, $f = 1.0$, $\gamma = 0.075$, $\Gamma = 1.0$, $\mathbf{Z}(0) = (X(0), \dot{X}(0), Y(0))^T = (0, 1, 0)^T$. Here we use the dimensionless version of our parameters, which is explicitly shown in Section 3.2. (a) X oscillates with a constant frequency ω_X after relaxing. (b) Y evolves linearly with the slope ω_Y.

$$\begin{aligned} \dot{\varphi} &= -\frac{\gamma}{2}\tan(\varphi_0 - \theta_0) \\ \dot{\theta} &= -\frac{\kappa^2}{2\Gamma\gamma\omega}\cos^2(\varphi_0 - \theta_0) \\ A &= -\frac{\kappa}{\gamma\omega}\cos(\varphi_0 - \theta_0). \end{aligned} \tag{2.17}$$

An equation for $\chi := \tan(\varphi_0 - \theta_0)$ is given by the synchronisation of the frequencies of X and Y, where we can insert $\dot{\varphi}$ and $\dot{\theta}$ and obtain a cubic equation

$$\chi^3 + \frac{2}{\gamma}(\omega' - \omega)\chi^2 + \chi + \frac{2}{\gamma}(\omega' - \omega) - \frac{\kappa^2}{\Gamma\gamma^2\omega} = 0. \tag{2.18}$$

If the cubic equation has one real root, it is automatically stable. If it instead has three real roots, then one of them is unstable and there are hysterese effects[3].

In the analytical approach to Eq. (2.10), we have made approximations whose reasonableness is to be verified numerically. This can be done by performing numerical simulations of the problem using the **forward Euler method**, which works by dividing the time into small steps of length δ. A more detailed explanation of the method is given in Ch. 3. As shown in Fig. 2.5, we find that X settles into a stable oscillation after a particular relaxation time while Y shows a linear trajectory, fulfilling their purposes as an oscillator and a counter[4].

[3]The nature of the roots can be determined by using the discriminant, which is beyond the scope of this thesis.

[4]Note that a long relaxation time indicates a stable system.

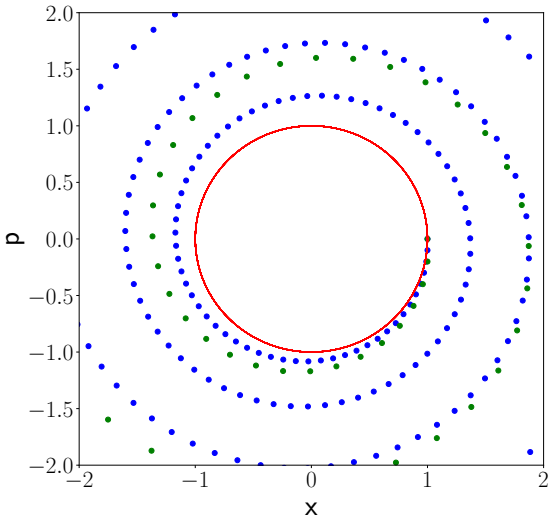

Figure 2.6: Visualization of the accumulation of errors in the simulation of the simple harmonic oscillator using a step length of $\delta_{\text{blue}} = 0.1$, $\delta_{\text{green}} = 0.2$, $A = 1.0$ and $\omega = 1.0$. The blue and green dots represent the numerical solution using the forward Euler method and the red line represents the analytical solution.

While the forward Euler method is one of the simplest ways of approximating a differential equation, it also tends to be subject to some errors. Especially the harmonic oscillator and systems containing such can be challenging to simulate if the step length δ is not sufficiently small. As shown in Fig. 2.6, where the accumulation of errors in the forward Euler method is depicted for different values of δ, the numerical solution converges to the analytical solution using smaller and smaller discretisation steps. Our system encounters similar problems, although they are less apparent.

Looking at the force dependency of the amplitude $A(f)$ and the oscillation frequency $\omega_{X/Y}(f)$ in the clock circuit and comparing the analytical and numerical solutions, we find similar results. The graphs are depicted in Fig. 2.7. Around $f = 1$, the point where the natural frequencies of both parts of the circuit align, meaning $\omega = \omega'$, the amplitude of the X oscillation has its peak. Furthermore, the slope of $\omega_{X/Y}(f)$ reaches a minimum. Here, we find a more stable region where if the force is ever not constant but exposed to noise, the fluctuations of the oscillation frequency are reduced.

When we look at the quality of the results, we see that while the analytical and numerical approaches both arrive at roughly the same frequencies, they deliver

slightly different amplitudes. Here, we encounter some errors in both methods, either caused by approximations we made or shortcomings of the simulations. In the analytical approach, we assumed X to be small, which is valid as long as we are far from $f = 1$. Still, the deviation from the numerics is slight enough to continue with this approach. It is also apparent that similar to the case of the harmonic oscillator, the numerical solution converges. From here on, all simulations of the clock circuit will be run with a discretization value of $\delta = 0.001$, which is both small enough to still be decently accurate and large enough to keep the runtime of the simulations reasonable.

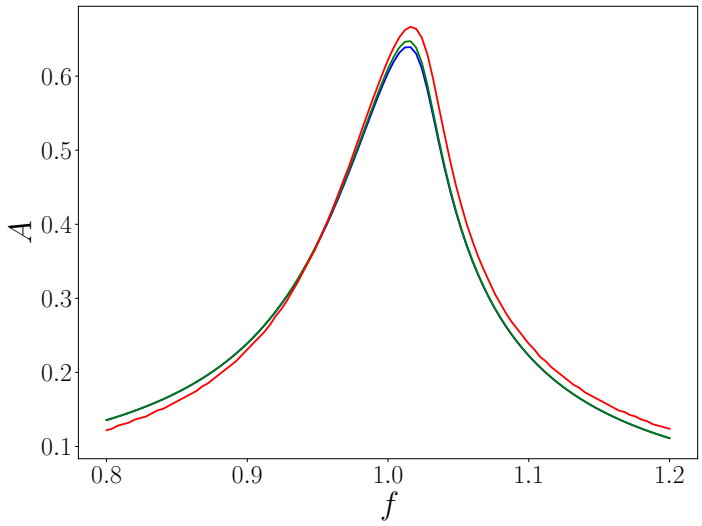

(a)

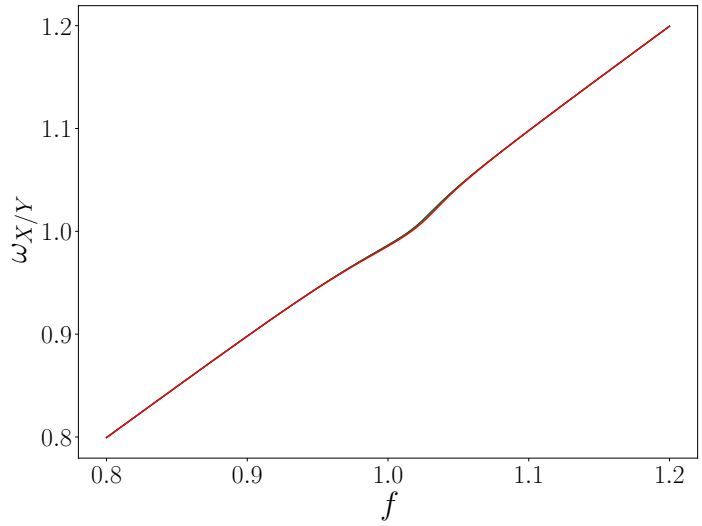

(b)

Figure 2.7: Numerical and analytical simulations of A and $\omega_{X/Y}$ with $\kappa = 0.05$, $\gamma = 0.075$ and $\Gamma = 1.0$. (a) Amplitude $A(f)$ of X. The red line represents the analytical solution, while green and blue represent the numerical solutions with $\delta_{\text{green}} = 0.002$ and $\delta_{\text{blue}} = 0.001$. (b) Frequency $\omega_{X/Y}(f)$. The colour representation stays the same.

Chapter 3

Influence of thermal noise

Up until this point, we have discussed the AC Josephson effect and the clock circuit at zero temperatures. As this is not a realistic scenario, we now introduce the influence of thermal noise and investigate the stability of the Josephson radiation emitted by both circuits.

3.1 Introduction to Johnson-Nyquist noise

A general noise signal can be described by a statistical variable $\xi(t)$ with a mean of $\langle \xi(t) \rangle = 0$ and the autocorrelation function

$$\langle \xi(t)\xi(t') \rangle = f(t - t'), \tag{3.1}$$

where $\langle \cdot \rangle$ denotes the average of the statistical ensemble [10]. Another way of defining the noise is given by the representation in the Fourier space

$$\langle \xi^*(\omega)\xi(\omega') \rangle = 2\pi S(\omega)\delta(\omega + \omega'), \tag{3.2}$$

where the spectral density $S(\omega)$ is the Fourier transform of the autocorrelation function[1] [10]

$$S(\omega) = \int_{-\infty}^{\infty} dt\, e^{i\omega t} f(t), \qquad f(t) = \frac{1}{2\pi} \int_{-\infty}^{\infty} d\omega\, e^{-i\omega t} S(\omega). \tag{3.3}$$

We will focus on the Johnson-Nyquist noise, which is caused by the thermal motion of the charge carriers in an electrical conductor at equilibrium. It is independent of the applied voltage and, therefore, also provides a contribution when $V = 0$. Furthermore, the Johnson-Nyquist noise is a white noise with a

[1] Note that we define the spectral density for both positive and negative frequencies.

Spectral density that is constant over the entire Fourier space[2] $S(\omega) \equiv S(0)$. Thus, the autocorrelation function for a statistical current δI with $\langle \delta I \rangle = 0$ is given by

$$\langle \delta I(t) \delta I(t') \rangle = f(t - t') = \alpha \, \delta(t - t'). \tag{3.4}$$

We can determine the prefactor α by calculating the energy in an example circuit. A noise current contribution for a resistor in any circuit can be modelled by considering a noiseless resistor at temperature $T = 0$ and adding a statistical current source in parallel[3]. With this, the circuit we want to examine consists of a resistor at zero temperature, parallel to a current source δI and an inductance L. It is depicted in Fig. 3.1. The equation of motion for the current in such a setup is given by

$$I + \frac{L}{R} \dot{I} = \delta I, \tag{3.5}$$

with $I(0) = 0$. We can solve the homogeneous differential equation first and then include the noise term to determine the inhomogeneous solution, which leads us to the following integral

$$I(t) = \frac{R}{L} e^{-\frac{R}{L}t} \int_0^t dt' \delta I(t') e^{-\frac{R}{L}t}. \tag{3.6}$$

Now the order of calculating the integral and the ensemble average can be swapped and the average current equates to $\langle I(t) \rangle = 0$. The same can be done for the autocorrelation function, yielding

$$\begin{aligned} \langle I^2(t) \rangle &= \left(\frac{R}{L} \right)^2 e^{-2\frac{R}{L}t} \int_0^t dt' \int_0^t dt'' \langle \delta I(t') \delta I(t'') \rangle e^{\frac{R}{L}t'} e^{\frac{R}{L}t''} \\ &= \alpha \frac{R}{2L} \left(1 - e^{-2\frac{R}{L}t} \right). \end{aligned} \tag{3.7}$$

In the limit $t \to \infty$, the energy in the circuit has to fulfil the equipartition theorem given by $E = \frac{L\langle I^2 \rangle}{2} = \frac{k_B T}{2}$, with the Boltzmann constant k_B. By comparison with Eq. (3.7) we obtain $\alpha = \frac{2 k_B T}{R}$. This is a manifestation of the fluctuation-dissipation-theorem, which states that a current flowing through a resistor dissipates electric energy, turning it into heat. The Johnson-Nyquist noise has the inverted effect of turning heat back into electric energy.

[2] In reality, Johnson-Nyquist noise decays to zero at extremely high frequencies (THz for room temperature) [11]. We are not interested in this regime, though.

[3] This is called the Norton equivalent circuit.

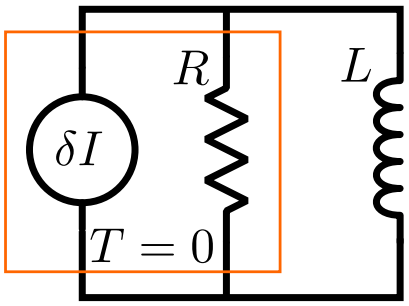

Figure 3.1: Circuit with a resistor at nonzero temperature, modelled by a resistor at zero temperature in parallel with a noise current source $\delta I(t)$ and shunted by a constant inductance. The energy stored in the magnetic field of the inductance is given by $E = \frac{L\langle I^2\rangle}{2}$.

3.2 Numerical approach with a noise term

We use the **forward Euler method** for the numerical simulation of the Josephson and the clock circuit. For this, the time is discretised using small steps of length δ. The solution of a general first order differential equation $\mathbf{Z}(t) = \mathbf{f(t,\ Z(t))}$ is then estimated by approximating the force at a certain point in time $\mathbf{f(t,\ Z(t))} \approx \mathbf{f}(t_0, \mathbf{Z}(t_0))$ for $t \in [t_0, t_0 + \delta]$ [12] and calculating the derivative $\dot{\mathbf{Z}}(t)$ by use of the differential quotient

$$\dot{\mathbf{Z}}_j \approx \frac{\mathbf{Z}_{j+1} - \mathbf{Z}_j}{\delta} = \mathbf{f}(\mathbf{Z}_j, t_j) \Rightarrow \mathbf{Z}_{j+1} = \mathbf{Z}_j + \delta \mathbf{f}(\mathbf{Z}_j, t_j), \tag{3.8}$$

where the time t_j after j integration steps is given by $t_0 + j\delta$. This approximation works well when the change of force happens on larger time scales than δ. Thus, the quality of such a simulation can be improved by choosing smaller discretisations or finding parameters that lead to a more stable system. In turn, the smaller δ is, the longer the simulation takes to run, which can often be impractical. In the case of the realistic Josephson circuit, $\mathbf{Z}$ is simply given by the superconducting phase $Z = \varphi$, while the clock circuit can be simulated using $\mathbf{Z} = (X, \dot{X}, Y)^T$, which recontextualises the second-order derivative in the differential equation as a first-order derivative of the variable $\dot{X}$.

For all numerical simulations, it is essential to convert the differential equations into a dimensionless form. This can be achieved by introducing the time scale $\tau = \omega t$ with $\omega = \sqrt{\frac{1}{LC}}$ and transforming the parameters we defined in Section 2.3 to find

$$\kappa = \frac{2eZ_0 I_c}{\hbar\omega},\ f = \kappa\frac{I_0}{I_c},\ \gamma = \frac{Z_0}{R_{LC}},\ \Gamma = \frac{Z_0}{R}.$$

Now the system of differential equations (Eq. (2.12)) still holds for the clock circuit, but with the new frequency $\tilde{\omega} = 1$. To obtain a more stable simulation, it is also helpful to rewrite the oscillating terms in the equation describing the motion of the current in the upper branch. Thus, we simulate the clock circuit

using

$$\kappa \sin(Y - X) = \ddot{X} + \tilde{\omega}^2 X + \gamma \dot{X} \tag{3.9a}$$

$$\Gamma \dot{Y} = f + 2\kappa \sin\left(\frac{X}{2}\right) \cos\left(Y - \frac{X}{2}\right). \tag{3.9b}$$

Similarly, the differential equation for the Josephson circuit in dimensionless form is given by

$$\Gamma \dot{\varphi} = f - \kappa \sin(\varphi), \tag{3.10}$$

which closely resembles the second equation of the clock circuit.

We now introduce the implementation of a white noise term by considering a general stochastic differential equation $\dot{X} = \xi(t)$ with $X(0) = 0$, $\langle \xi(t) \rangle = 0$ and $\langle \xi(t)\xi(t') \rangle = \alpha\, \delta(t - t')$. The time evolution of X is then given by

$$\begin{aligned} X_{j+1} &= X_j + \int_{t_j}^{t_{j+1}} dt \dot{X}(t) \\ &= X_j + \delta\, \xi_j. \end{aligned} \tag{3.11}$$

Using the same method of evaluating the ensemble average before the integral as we did in Eq. (3.7), we can also calculate the time evolution of the autocorrelation function analytically, yielding

$$\langle X^2(t) \rangle = \int_0^t dt' \int_0^t dt'' \langle \xi(t')\xi(t'') \rangle = \alpha\, t. \tag{3.12}$$

Thus, the contribution of the noise term can be modelled by defining a statistical variable that is zero on average and has a variance of $\sigma^2 = \alpha\ t$. The easiest way of doing so is through the use of a normally distributed random variable $\xi_j(t)$ with a mean of $\mu_{\xi_j} = 0$ and a standard deviation of $\sigma_{\xi_j} = \sqrt{\frac{\alpha}{\delta}}$. Hereby, we excluded the extra factor of δ coming from the Forward Euler method.

3.3 First-order coherence

The **first-order coherence** quantifies the coherence between two electric fields, which can be measured using an interferometer. Thus, it is a way to determine the stability of the Josephson radiation emitted by the two circuits introduced in Ch. 2 under the influence of thermal noise. For plane parallel waves with

the field vector $E(t)$, the normalized first-order correlation function is given by

$$g^{(1)}(\tau) = \frac{\langle E^*(t)E(t+\tau)\rangle}{\langle |E(t)|^2\rangle}, \tag{3.13}$$

where $\langle\cdot\rangle$ denotes an ensemble average. Here, we assume the system emitting the radiation to be in a stationary state, meaning its statistical properties do not change with time. Therefore, $g^{(1)}(\tau)$ does not depend on the time itself, which can be set to zero. It instead measures the coherence of the radiation at two different points in time separated by the delay τ. Using the variable transformation $t \to t' = t - \tau$ and the fact that the field vectors commute, we can deduce that $g^{(1)}(\tau)$ is an even function.

Since we are considering oscillating variables, it makes sense to transition into their respective rotating frames and observe the physics from this point of view. The rotating frame can be constructed by starting with a general oscillating variable $X = Re(\alpha e^{-i\omega t})$ with the frequency ω and the amplitude $\alpha = Ae^{-i\varphi}$, which depends on the constant amplitude $A \in \mathbb{R}$ and a slow phase $\varphi(t)$. From there, we can switch into observing α using the transformation $\alpha = e^{i\omega t}\left(X + i\frac{\dot{X}}{\omega}\right)$. The first-order coherence is then given by

$$g^{(1)}(\tau) = \frac{\langle \alpha^*(\tau)\alpha(0)\rangle}{\langle |\alpha(0)|^2\rangle}. \tag{3.14}$$

In the case of an ideal laser, the radiation is always fully coherent, which is expressed by $g^{(1)} = 1$, independent of the delay τ. We expect this to be the case for both circuits at zero temperature. In the opposite case, fully incoherent light has a first-order coherence value of $g^{(1)} = 0$, while all other light sources with $0 < g^{(1)} < 1$ are called partially coherent.

3.4 Radiation coherence in the Josephson circuit

At non-zero temperatures, the equation of motion for the current in the Josephson circuit, which is depicted in Fig. 3.2, can be obtained using Kirchhoff's current law

$$I_0 + \delta I = I_c \sin(\varphi) + \frac{1}{\tilde{R}}\dot{\varphi}. \tag{3.15}$$

Here, we stay within the low-temperature limit, assuming the statistical current δI, which is both random and deterministic, to fulfil $\delta I \ll I_0$. Analogous to Ch. 2, where we determined the solution to the non-statistical differential equation, the contribution of the capacitor in the RCSJ model is neglected and

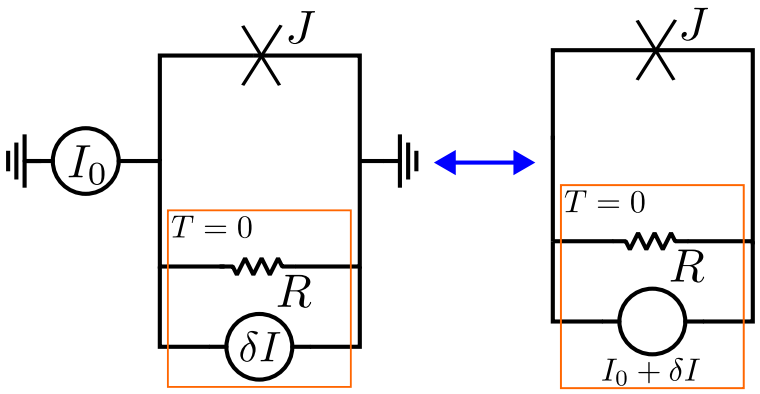

Figure 3.2: Schematic depiction of the Josephson circuit under the influence of thermal noise. It is modelled by adding a current source δI in parallel to the resistor. The left and the right depiction of the circuit are equivalent, meaning we can summarise the current sources.

the supplied DC current is assumed to be much larger than the critical current of the junction. Now the statistical differential equation can be solved by using the method of variation of parameters. We thus give a time-dependeny to the constant of integration in the homogeneous solution for the superconducting phase (Eq. (2.7)), i.e. $\theta = \frac{\omega_0 t_0}{2} \rightarrow \theta(t)$ with $\theta(0) = 0$. $\varphi(t, \theta(t))$ is then a function of the time itself, and a slow phase

$$\varphi(t, \theta(t)) = 2 \arctan\left(\frac{I_0 + I_c}{\sqrt{I_0^2 - I_c^2}} \tan\left(\frac{\omega_0 t + \theta(t)}{2}\right)\right) - \frac{\pi}{2}. \tag{3.16}$$

Inserting this into the statistical equation of motion for the current cancels the homogeneous solution and leaves us with

$$F\dot{\theta} = \frac{1}{\tilde{R}} \frac{\sqrt{I_0^2 - I_c^2}}{I_0 - I_c \cos(\omega_0 t + \theta)} \dot{\theta} = \delta I, \tag{3.17}$$

where $F(t, \theta(t))$ is a time-dependent force. By dividing both sides of the equation by F and integrating over θ and t respectively, we can find an expression for the additional phase. The force, and therefore its inverse, has both a constant and an oscillating component. To find out how the components contribute towards the noise current, we calculate the Fourier transform of F^{-1}. Under the assumption, that $\theta(t)$ is slow, such that it changes over much larger time scales than ω_0^{-1}, we can approximate it as a constant in the cosine and the Fourier

transform is trivial

$$\mathfrak{F}\{F^{-1}(t)\} = \frac{\tilde{R}}{\sqrt{I_0^2 - I_c^2}}\left[I_0\delta(\omega) - \frac{I_c}{2}\left(e^{i\theta_0}\delta(\omega-\omega_0) + e^{-i\theta_0}\delta(\omega+\omega_0)\right)\right]. \tag{3.18}$$

Since the spectral density of the thermal noise is constant in the Fourier space[4], the product of the inverse of the force and the noise current gives a contribution for every frequency in $F^{-1}(\omega)$, i.e. $\omega = 0, +\omega_0, -\omega_0$. Moreover, we define δI to also be evenly distributed in the complex plane, meaning it negates the phases coming from θ_0. Thus, we find that the resulting thermal noise is of the form

$$F^{-1}(t)\delta I(t) = \tilde{R}\sqrt{\frac{I_0 - I_c}{I_0 + I_c}}\delta I(t), \tag{3.19}$$

where the AC part of the force has been downconverted. θ now fulfils the simple statistical differential equation $\dot{\theta} = \delta I'$, where the modified noise current still has a mean of zero and a new standard deviation defined by $\sigma^2_{\delta I'} = \frac{I_0 - I_c}{I_0 + I_c}\varepsilon$, yielding $\langle\theta(t)\rangle = 0$ and $\langle\theta^2(t)\rangle = \frac{I_0 - I_c}{I_0 + I_c}\varepsilon t$. Here we introduce the parameter $\varepsilon(T) = \frac{8e^2R}{\hbar^2}k_BT$, which is linearly dependent on the temperature and controls the amplitude of the noise signal.

Ignoring higher frequencies, the rotating frame is given by $\alpha = Ae^{-i\theta(t)}$. Inserting this into Eq. (3.14) yields $g^{(1)}(\tau) = \langle e^{i\theta(\tau)}\rangle$. In general, if a random variable X has a density function p, the expected value of a function $f(X)$ can be calculated using $\langle f(X)\rangle = \int_{-\infty}^{\infty} dx f(x)p(x)$. By assuming θ to be a normally distributed random variable with $\mu = 0$ and $\sigma^2 = \sigma^2_{\delta I'}t$, we can calculate the first-order coherence

$$\begin{aligned} g^{(1)}(\tau) &= \int_{-\infty}^{\infty} d\theta e^{-i\theta}\frac{1}{\sigma\sqrt{2\pi}}e^{-\frac{\theta^2}{2\sigma^2}} \\ &= e^{-\frac{\sigma^2}{2}}\int_{-\infty}^{\infty} d\theta \frac{1}{\sigma\sqrt{2\pi}}e^{-\frac{(\theta+i\sigma^2)^2}{2\sigma^2}} \\ &= e^{-\frac{\sigma^2}{2}} \\ &= e^{-\frac{I_0 - I_c}{I_0 + I_c}\frac{\varepsilon}{2}\tau} \\ &\approx e^{-\frac{\varepsilon}{2}\tau}, \end{aligned} \tag{3.20}$$

where in the last step we insert the assumption $I_0 \gg I_c$. As expected, $g^{(1)} = 1$ for zero temperature, independent of the delay. The only other way to get fully coherent light is to reduce the resistance to zero. This is equivalent to the

[4]The noise current is in this case essentially given by $\delta I(t) = \delta I_0(t) + \mathrm{Re}\left(I_1(t)e^{-i\omega_0 t}\right) + \mathrm{Re}\left(I_2(t)e^{i\omega_0 t}\right)$. Multiplying with $F^{-1}(t)$ yields the downconversion and a negligible AC part.

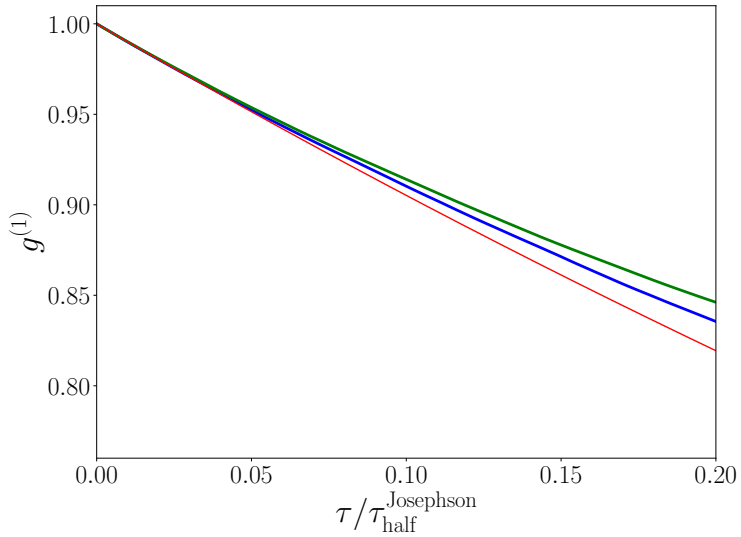

Figure 3.3: First-order coherence of the radiation emitted by the Josephson circuit with $f = 5.0$, $\Gamma = 1.0$, $\kappa = 0.01$ and $\varepsilon = 5 \cdot 10^{-5}$. The analytical result is shown in red, while the numerical results are shown in green and blue. The numerical results have both been achieved using a step length of $\delta = 0.005$ with different integration times $t_{\text{int}}^{\text{green}} = 60000$ and $t_{\text{int}}^{\text{blue}} = 80000$.

case of the ideal Josephson circuit, which we already identified as unrealistic. Finally, we can identify the half-life of the first-order coherence as a measure of stability of the emitted Josephson radiation

$$\boxed{g^{(1)}(\tau_{\text{half}}^{\text{Josephson}}) = e^{-1} \Rightarrow \tau_{\text{half}}^{\text{Josephson}} = \frac{2}{\varepsilon}.} \tag{3.21}$$

A comparison between the analytical result and the numerical result is shown in Fig. 3.3. For the numerics, we simulate 1000 samples using the statistical differential equation, translate each of them into the rotating frame, and then correlate the samples using the scipy function "signal.correlate". We see that for small delays, the analytical and the numerical results match. For longer delays, the numerical simulation results in a more stable oscillation than what the analytics show. However, the longer the integration period is with which we simulate each sample, the more the numerical result converges towards the analytical result, which is likely because the correlate function has a higher number of input values, the longer the interval is that is being correlated. Thus, while we made approximations in both methods, we assume that for long enough simulations, they arrive at a similar first-order coherence.

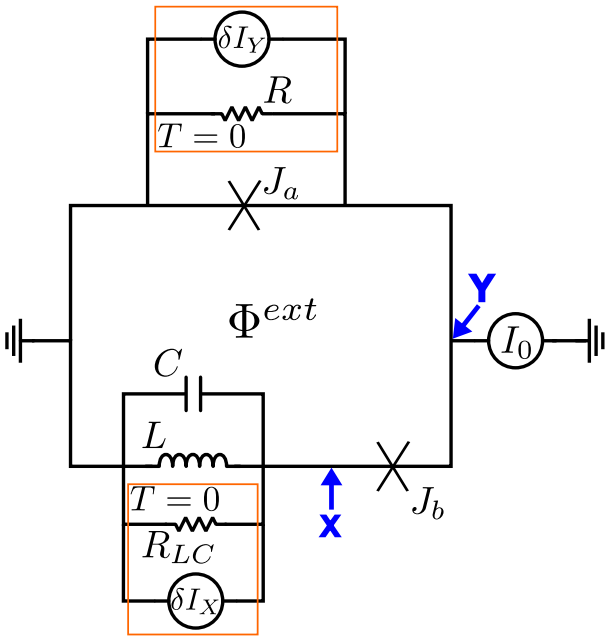

Figure 3.4: Schematic depiction of the clock circuit under the influence of thermal noise. The lower branch is extended by the noise current δI_X parallel to R_{LC}, the upper branch gains a noise current δI_Y parallel to R.

3.5 Radiation coherence in the clock circuit

We now want to take a look at the stability of the Josephson radiation emitted by the clock circuit at finite temperatures and compare it to the simple Josephson circuit. Using Kirchhoff's current law and implementing the parameters defined in Section 2.3, the system of statistical differential equations is given by

$$\kappa \sin(Y - X) = \ddot{X} + \omega^2 X + \dot{X} + \kappa \frac{\delta I_X}{I_c} \tag{3.22a}$$

$$f = \Gamma \dot{Y} + \kappa \sin(Y + \pi) + \kappa \sin(Y - X) + \kappa \frac{\delta I_Y}{I_c}, \tag{3.22b}$$

with an additional noise current in both the upper and the lower branch. A representation of the circuit is shown in Fig. 3.4. Assuming the temperature of both resistors to be equal, the noise currents then satisfy $\langle \delta I_X(t) \rangle = \langle \delta I_Y(t) \rangle = 0$ and

$$\begin{aligned} \langle \delta I_X(t) \delta I_X(t') \rangle &= \frac{2 k_B T}{R_{LC}} \delta(t - t') \\ \langle \delta I_Y(t) \delta I_Y(t') \rangle &= \frac{2 k_B T}{R} \delta(t - t'), \end{aligned} \tag{3.23}$$

respectively. The autocorrelation functions only differ by a factor of $\frac{R}{R_{LC}} = \frac{\gamma}{\Gamma}$, wherefore we can express the currents by noise of equal amplitude with a different prefactor $\delta I_Y = \delta I_2$ and $\delta I_X = \sqrt{\frac{\gamma}{\Gamma}}\delta I_1$. Here δI_1 and δI_2 have the same means and standard deviations but are uncorrelated statistical variables. In order to describe Eq. (3.22) analytically, we extend our ansatz for X and Y from Eq. (2.13) by adding the small, slow, time-dependent phases $\varphi_1(t)$ and $\theta_1(t)$

$$\begin{aligned} X(t) &= \mathrm{Re}\left(Ae^{-i(\omega t+\varphi(t)+\varphi_1(t))}\right) \\ Y(t) &= \omega' t + \theta(t) + \theta_1(t). \end{aligned} \tag{3.24}$$

The approximations we made in Ch. 2 for the non-statistical differential equations can now be utilised again to find expressions for the additional phases. For Eq. (3.22a), this means omitting small terms of $\mathcal{O}\left(\dot{\varphi}^2\right)$, $\mathcal{O}\left({\dot{\varphi_1}}^2\right)$, $\mathcal{O}\left(\gamma\dot{\varphi}\right)$ and $\mathcal{O}\left(\gamma\dot{\varphi_1}\right)$. We then find an equation for $\dot{\varphi}_1$, where, assuming $(\varphi_1 - \theta_1)$ to be small, the oscillating sine term can be first order taylor expanded to find

$$\begin{aligned} \dot{\varphi}_1 &= \frac{\kappa}{2A\omega}\left[\sin(\varphi_0 - \theta_0 + \varphi_1 - \theta_1) + \sqrt{\frac{\gamma}{\Gamma}}\frac{\cos(\omega t + \varphi + \varphi_1)}{I_c}\delta I_1\right] - \dot{\varphi} \\ &\approx \frac{\kappa}{2A\omega}\left[\sin(\varphi_0 - \theta_0) + \cos(\varphi_0 - \theta_0)(\varphi_1 - \theta_1) + \sqrt{\frac{\gamma}{\Gamma}}\frac{\cos(\omega t + \varphi + \varphi_1)}{I_c}\delta I_1\right] - \dot{\varphi} \\ &= \frac{\kappa}{2A\omega}\left[\cos(\varphi_0 - \theta_0)(\varphi_1 - \theta_1) + \sqrt{\frac{\gamma}{\Gamma}}\frac{\cos(\omega t + \varphi + \varphi_1)}{I_c}\delta I_1\right]. \end{aligned} \tag{3.25}$$

A similar procedure yields an expression for θ_1. As in Ch. 2, we use the rotating wave approximation to get rid of the fast oscillating terms and first order taylor expand the cosine, obtaining

$$\begin{aligned} \dot{\theta}_1 &= \frac{\kappa A}{2\Gamma}\cos(\varphi_0 - \theta_0 + \varphi_1 - \theta_1) - \frac{\kappa}{\Gamma I_c}\delta I_2 - \dot{\theta} \\ &\approx \frac{\kappa A}{2\Gamma}\left[\cos(\varphi_0 - \theta_0) - \sin(\varphi_0 - \theta_0)(\varphi_1 - \theta_1)\right] - \frac{\kappa}{\Gamma I_c}\delta I_2 - \dot{\theta} \\ &= -\frac{\kappa A}{2\Gamma}\sin(\varphi_0 - \theta_0)(\varphi_1 - \theta_1) - \frac{\kappa}{\Gamma I_c}\delta I_2. \end{aligned} \tag{3.26}$$

The new differential equations for the additional phases both have a part that depends on the phase difference $(\varphi_1 - \theta_1)$ as well as a noise term. We can express this as the matrix

$$\begin{pmatrix}\dot{\varphi}_1 \\ \dot{\theta}_1\end{pmatrix} = \begin{pmatrix}-a & a \\ b & -b\end{pmatrix}\begin{pmatrix}\varphi_1 \\ \theta_1\end{pmatrix} + \begin{pmatrix}\alpha\beta\cos(\omega_X t + \varphi_0 + \varphi_1) & 0 \\ 0 & \beta\end{pmatrix}\begin{pmatrix}\delta I_1 \\ \delta I_2\end{pmatrix}, \tag{3.27}$$

with the following parameters

$$\begin{aligned} a &= \frac{\gamma}{2} \\ b &= \frac{\kappa^2}{2\gamma\Gamma\omega}\cos(\varphi_0-\theta_0)\sin(\varphi_0-\theta_0) \\ \alpha &= \frac{\gamma}{2\kappa}\frac{\sqrt{\gamma\Gamma}}{\cos(\varphi_0-\theta_0)} \\ \beta &= -\frac{\kappa}{\Gamma I_c}. \end{aligned} \tag{3.28}$$

The non-statistical homogeneous part can easily be solved by finding the eigenvalues and eigenvectors to diagonalize the matrix. For a time-independent matrix $\mathbf{A}$ with n linearly independent eigenvectors $\mathbf{v}$, the general solution for a first-order matrix differential equation $\dot{\mathbf{z}}(t) = \mathbf{A}\mathbf{z}(t)$ is given by $\mathbf{z} = c_1 e^{\lambda_1 t}\mathbf{v}_1 + c_2 e^{\lambda_2 t}\mathbf{v}_2 + ... + c_n e^{\lambda_n t}\mathbf{v}_n$ [13]. In our case, this yields

$$\begin{pmatrix}\varphi_1 \\ \theta_1\end{pmatrix} = c_1\begin{pmatrix}1 \\ 1\end{pmatrix} + c_2 e^{-(a+b)t}\begin{pmatrix}-\frac{a}{b} \\ 1\end{pmatrix}. \tag{3.29}$$

To solve the statistical part, we choose the integration constants c_1 and c_2 to be time-dependent and find two new equations

$$\begin{aligned} \dot{c_1}(t) &= \frac{a}{a+b}\left[\alpha\beta\frac{b}{a}\cos(\omega_X t+\varphi_0+\varphi_1(t))\delta I_1(t)+\beta\delta I_2(t)\right] \\ \dot{c_2}(t) &= \frac{b}{a+b}e^{(a+b)t}\Big[-\alpha\beta\cos(\omega_X t+\varphi_0+\varphi_1(t))\delta I_1(t)+\beta\delta I_2(t)\Big], \end{aligned} \tag{3.30}$$

that both include a constant and an oscillating part. As for the Josephson circuit, the downconversion of the oscillating term yields an additional contribution to the noise current. Since $\varphi_1(t)$ is a slow variable compared to ω_X^{-1}, we approximate its contribution in the cosine to be constant and the derivation of the downconversion is analogous to the case of the Josephson circuit. This leaves us with

$$\begin{aligned} c_1(t) &= \frac{a}{a+b}\int_0^t dt'\left[\alpha\beta\frac{b}{a}\delta I_1(t')+\beta\delta I_2(t')\right] \\ c_2(t) &= \frac{b}{a+b}\int_0^t dt' e^{(a+b)t'}\Big[-\alpha\beta\delta I_1(t')+\beta\delta I_2(t')\Big], \end{aligned} \tag{3.31}$$

which in turn defines $\varphi_1 = c_1 - \frac{a}{b}c_2 e^{-(a+b)t}$. We are especially interested in φ_1, because it is the time-dependent phase in the rotating frame $\alpha = Ae^{-i\varphi_1}$.

Thus, in order to calculate $g^{(1)}$, we need the variance of φ_1, which is given by

$$\langle\varphi_1^2\rangle = \langle c_1^2\rangle - 2\frac{a}{b}\langle c_1 c_2\rangle e^{-(a+b)t} + \left(\frac{a}{b}\right)^2 \langle c_2^2\rangle e^{-2(a+b)t}. \tag{3.32}$$

We can calculate each correlation function separately. Starting with

$$\begin{aligned}\langle c_1^2\rangle &= \left(\frac{a}{a+b}\right)^2 \left\langle \left[\alpha\beta\frac{b}{a}\int dt'\delta I_1(t') + \beta\int dt''\delta I_2(t'')\right]^2\right\rangle \\ &= \left(\frac{a}{a+b}\right)^2 \left[\left(\alpha\beta\frac{b}{a}\right)^2 \int_0^t dt'' \int_0^t dt' \langle\delta I_1(t')\delta I_1(t'')\rangle \right. \\ &\qquad \left. + \beta^2 \int_0^t dt'' \int_0^t dt' \langle\delta I_2(t')\delta I_2(t'')\rangle\right] \\ &= \frac{a^2+\alpha^2 b^2}{(a+b)^2}\varepsilon t,\end{aligned} \tag{3.33}$$

where we summarised $\beta^2\frac{2k_BT}{R} = \varepsilon$. The mixed term with contributions of both noise currents vanishes because the random variables are uncorrelated. Similar to this first expectation value, the other parts of $\langle\varphi_1^2\rangle$ can be derived, which is shown App. A. The results are

$$\langle c_1 c_2\rangle e^{-(a+b)t} = \frac{ab}{(a+b)^3}\left[1-\alpha^2\frac{b}{a}\right]\left(1-e^{-(a+b)t}\right)\varepsilon \tag{3.34a}$$

$$\langle c_2^2\rangle e^{-2(a+b)t} = \frac{b^2}{2(a+b)^3}\left[1+\alpha^2\right]\left(1-e^{-2(a+b)t}\right)\varepsilon. \tag{3.34b}$$

After a short period of time, the contribution of the first correlation function will outweigh the others. We are interested in the long-term behaviour of the circuit, wherefore $\langle\varphi_1^2\rangle$ can be modelled by just $\langle c_1^2\rangle$ and we find a first-order coherence of

$$g^{(1)}(\tau) = e^{-\frac{a^2+\beta^2b^2}{(a+b)^2}\frac{\varepsilon}{2}\tau}. \tag{3.35}$$

A comparison between the analytical and the numerical solution is shown in Fig. 3.5. As with the Josephson circuit, the numerics result in a more stable first-order coherence than what the analytics suggest. Also similar to before, the numerical simulations converge towards the analytical solution for longer integration times. Furthermore, we see that the numerical solutions of the first-order coherence oscillate. The cause of this can be found in the transition to the rotating frame, where higher order frequencies are neglected. Moreover, we need to remember, that using the forward Euler method, the numerical calculations will always include errors. We aim to minimize them by choosing a small value of δ, but they should not be neglected. Lastly, the more stable the circuit

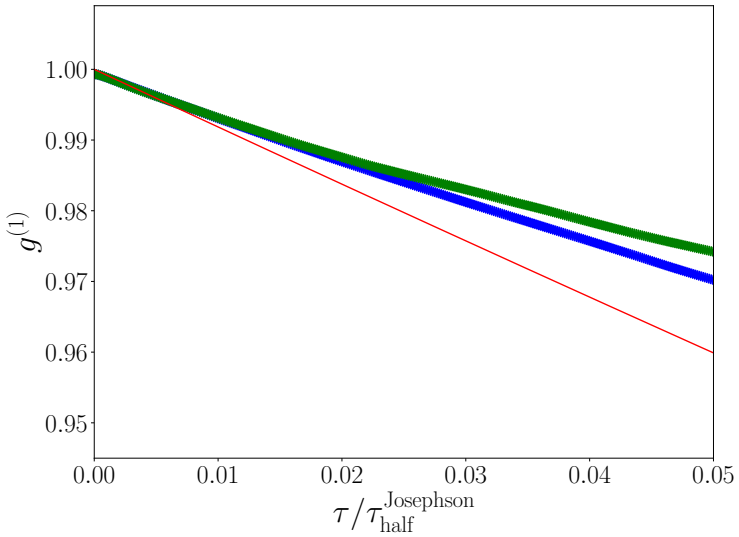

Figure 3.5: First-order coherence of the radiation emitted by the clock circuit with $\kappa = 0.05$, $\gamma = 0.075$, $\Gamma = 1$, $f = 1$ and $\varepsilon = 5 \cdot 10^{-5}$. The analytical result is shown in red, while the numerical results are shown in green and blue. The numerical results have both been achieved using a step length of $\delta = 0.001$ with different integration times $t_{\text{int}}^{\text{green}} = 11000$ and $t_{\text{int}}^{\text{blue}} = 21000$.

is, the longer the relaxation time becomes and it takes longer periods of time for X to settle into a stable oscillation from which we can go into the rotating frame, further complicating the attempt simulating the emission of radiation. In the end, it is not far-fetched to say, that the numerical simulations, while still in need of improvement, confirm that the approximations made to achieve the analytical solution are reasonable.

Lastly, we want to discuss how to improve the stability of the radiation. If the prefactor in the exponent of $g^{(1)}$ fulfils $\frac{a^2+\beta^2 b^2}{(a+b)^2} = 1$, the first-order coherence of the clock circuit is equal to that of the Josephson circuit. Thus, we are looking for parameters that reduce the prefactor. The half-life of the radiation emitted by the clock circuit compared to that of the Josephson circuit defines the improvement in stability S and is given by

$$S := \frac{\tau_{\text{half}}^{\text{clock}}}{\tau_{\text{half}}^{\text{Josephson}}} = \frac{1 + 2\frac{\kappa^2}{\gamma^2\Gamma\omega}\chi_1 + \frac{\kappa^4}{\gamma^4\Gamma^2\omega^2}\chi_1^2}{1 + \frac{\kappa^2}{4\gamma\Gamma\omega^2}\chi_2^2}, \tag{3.36}$$

where χ_1 and χ_2 only depend on the phase difference $(\varphi_0 - \theta_0)$

$$\chi_1 = \cos(\varphi_0 - \theta_0)\sin(\varphi_0 - \theta_0) \tag{3.37a}$$

$$\chi_2 = \sin(\varphi_0 - \theta_0). \tag{3.37b}$$

We can relate them back to $\chi = \tan(\varphi_0 - \theta_0)$, which we defined in the previous chapter (Eq. (2.18)). Assuming $\kappa/\gamma \gg 1$, meaning there is a strong coupling between both branches of the circuit and a weak damping of the oscillator, χ then scales with $\chi \approx \left(\frac{\kappa^2}{\Gamma\gamma^2\omega}\right)^{\frac{1}{3}}$, which leads to $\chi_1 \approx \left(\frac{\kappa^2}{\Gamma\gamma^2\omega}\right)^{-\frac{1}{3}}$ and $\chi_2 \approx 1$. Inserting this into Eq. (3.36), we obtain an approximate result given by

$$\boxed{S \approx \frac{4\omega^{\frac{2}{3}}}{\Gamma^{\frac{1}{3}}\kappa}\left(\frac{\kappa}{\gamma}\right)^{\frac{5}{3}}.} \tag{3.38}$$

This result presents us with a way to stabilize the Josephson radiation emitted by the clock circuit, which is by increasing the coupling between the oscillator and the counter and/or decreasing the damping of the oscillator. It is also apparent, that decreasing γ is more effective than increasing κ, as it scales with a power of $p_\gamma = 5/3$ instead of $p_\kappa = 2/3$.

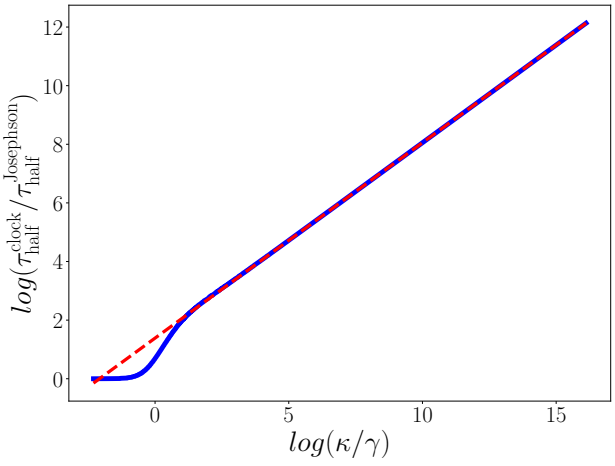

(a)

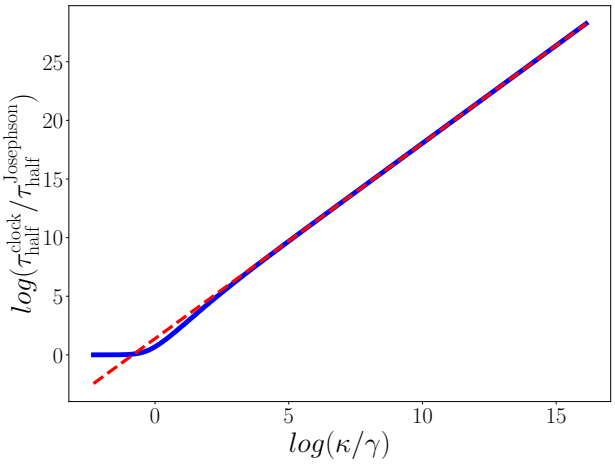

(b)

Figure 3.6: Logarithmic behaviour of Eq. (3.36) for large κ/γ with the dimensionless parameters $\Gamma = 1.0$ and $\tilde{\omega} = 1.0$. The exact result is shown in blue, while the red dotted line represents the approximate result derived in Eq. (3.38). a) Varying $\kappa \in [0.1, 10^7]$ with $\gamma = 1.0$ leads to a power law with power $p_\kappa = 2/3$. b) Varying $\gamma \in [10^{-7}, 10]$ with $\kappa = 1.0$ leads to a power law with power $p_\gamma = 5/3$.

Chapter 4

Conclusion and outlook

This thesis has dealt with the properties of radiation emitted by circuits that include Josephson junctions. The main focus has been quantifying the light's coherence while being emitted under the influence of Johnson-Nyquist noise.

In Ch. 2, we have introduced possible sources of Josephson radiation. First, we have discussed the ideal AC Josephson effect as a way of converting a supplied DC voltage to an outgoing AC current. Since it is impossible to realise an ideal voltage source, we have then introduced the RCSJ model and the realistic AC Josephson effect. Using this, we have built a circuit that utilises the aforementioned effect and functions as a clock with a counter and an oscillator.

The influence of thermal noise on both circuits has been discussed in Ch. 3. We have introduced the first-order correlation function as a way to measure the coherence of the Josephson radiation and found that, in the limit of large driving currents, the half-life of $g^{(1)}$ for the simple Josephson circuit is given by $\tau_{\text{half}}^{\text{Josephson}} = \frac{2}{\varepsilon}$, where $\varepsilon(T)$ is a parameter that linearly depends on the temperature. Then, we have shown that the clock circuit has the potential to improve the stability of the radiation significantly. The half-life of its first-order coherence is given by Eq. (3.36), which in the limit of strong coupling and weak damping of the oscillator, meaning $\kappa/\gamma \gg 1$, is $\tau_{\text{half}}^{\text{clock}} = \frac{4\omega^{\frac{2}{3}}}{\Gamma^{\frac{1}{3}}\kappa}\left(\frac{\kappa}{\gamma}\right)^{\frac{5}{3}}\frac{2}{\varepsilon}$. The optimal way of improving the half-life is thus given by weakening the damping symbolised by γ, as it scales with a power of $p_\gamma = 5/3$. Therefore, we have shown shown that there exists a circuit that can be tuned to emit light with specific coherence properties based on the given temperature.

The thesis took a first look at a clock circuit with promising results. However,

there is still room for further research. Mainly, the numerical approach needs to be improved, as we have shown that the forward Euler method is flawed. Due to it being very inaccurate for bigger step sizes and the clock circuit having longer relaxation times, the more stable the oscillation is, we could not simulate it with arbitrarily strong coupling and weak damping. Moreover, the entire thesis focused on the classical regime, ignoring quantum effects, which are yet to be included.

Appendix A

Calculation of negligible correlation functions

We now show the calculation of $\langle c_1 c_2 \rangle$ and $\langle c_2^2 \rangle$. Together with $\langle c_1^2 \rangle$, they define the variance of φ_1 in the clock circuit, which in turn is used to determine the first-order coherence. In both equations, we swap the evaluation of the ensemble average and the integral. We then see that the integrals containing correlation functions of the same noise current, meaning $\langle \delta I_{1/2}(t) I_{1/2}(t') \rangle = \frac{2k_B T}{R}$, yield a contribution. $\langle \delta I_1(t) I_2(t') \rangle = 0$ on the other hand can be dropped because the statistical variables are uncorrelated. For $\langle c_1 c_2 \rangle$ we find

$$\begin{aligned}
\langle c_1 c_2 \rangle =& \frac{ab}{(a+b)^2} \Bigg[-\alpha^2 \beta^2 \frac{b}{a} \int_0^t dt'' \int_0^t dt' e^{(a+b)t'} \langle \delta I_1(t'') \delta I_1(t') \rangle \\
&+ \beta^2 \int_0^t dt'' \int_0^t dt' e^{(a+b)t'} \langle \delta I_2(t'') \delta I_2(t') \rangle \\
&+ const. \int_0^t dt'' \int_0^t dt' e^{(a+b)t'} \langle \delta I_1(t'') \delta I_2(t') \rangle \Bigg] \\
=& \frac{ab}{(a+b)^2} \left[\left(1 - \alpha^2 \frac{b}{a} \right) \int_0^t dt'' \int_0^t dt' e^{(a+b)t'} \delta(t' - t'') \right] \varepsilon \\
=& \frac{ab}{(a+b)^2} \left[\left(1 - \alpha^2 \frac{b}{a} \right) \int_0^t dt'' e^{(a+b)t''} \right] \varepsilon \\
=& \frac{ab}{(a+b)^3} \left[1 - \alpha^2 \frac{b}{a} \right] \left(e^{(a+b)t} - 1 \right) \varepsilon,
\end{aligned} \tag{A.1}$$

which, when multiplied with $e^{-(a+b)t}$, is zero for $t = 0$ and for longer periods of time yields a contribution that can be neglected compared to $\langle c_1^2 \rangle$, as shown in

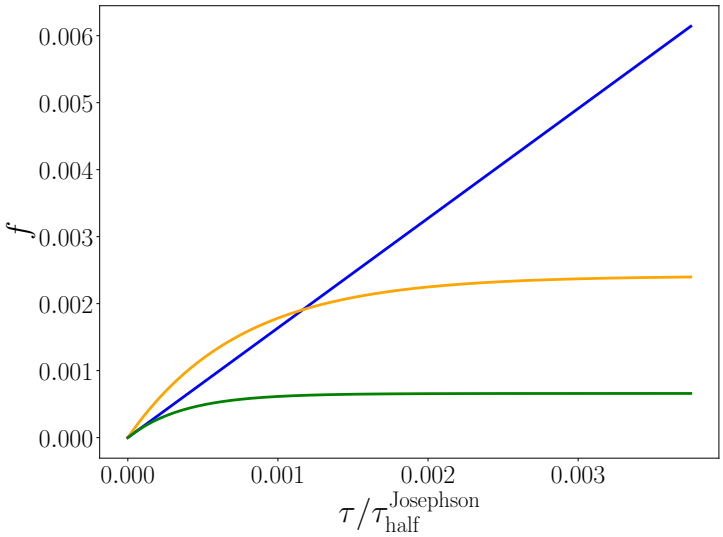

Figure A.1: Contributions f of the different autocorrelation functions towards $\langle\varphi_1^2\rangle$ with $\kappa = 0.05$, $\gamma = 0.075$, $\Gamma = 1.0$, $f = 1.0$ and $\varepsilon = 5 \cdot 10^{-5}$. $\langle c_1^2\rangle$, which is shown in blue, quickly outweighs $2\frac{a}{b}\langle c_1 c_2\rangle e^{-(a+b)t}$ and $\left(\frac{a}{b}\right)^2 \langle c_2^2\rangle e^{-2(a+b)t}$, shown in orange and green.

Fig. A.1. We evaluate a similar integral for the final autocorrelation function

$$\begin{aligned}
\langle c_2^2\rangle =& \frac{b^2}{(a+b)^2}\Bigg[\alpha^2\beta^2\int_0^t dt''\int_0^t dt' e^{(a+b)(t'+t'')}\langle\delta I_1(t'')\delta I_1(t')\rangle \\
&+ \beta^2\int_0^t dt''\int_0^t dt' e^{(a+b)(t'+t'')}\langle\delta I_2(t'')\delta I_2(t')\rangle \\
&+ const.\int_0^t dt''\int_0^t dt' e^{(a+b)(t'+t'')}\langle\delta I_1(t'')\delta I_2(t')\rangle\Bigg] \\
=& \frac{b^2}{(a+b)^2}\left[(1+\alpha^2)\int_0^t dt''\int_0^t dt' e^{(a+b)(t'+t'')}\delta(t'-t'')\right]\varepsilon \\
=& \frac{ab}{(a+b)^2}\left[(1+\alpha^2)\int_0^t dt'' e^{2(a+b)t''}\right]\varepsilon \\
=& \frac{b^2}{2(a+b)^3}\left[1+\alpha^2\right]\left(e^{2(a+b)t}-1\right)\varepsilon.
\end{aligned} \tag{A.2}$$

By multiplying with $e^{-2(a+b)t}$ and comparing with $\langle c_1^2\rangle$ in the limit of long delays, this result can be neglected as well.

Acknowledgements

I would like to thank Prof. Dr. Fabian Hassler for introducing me to this exciting branch of physics. His support was instrumental in the completion of this thesis.

I also want to thank David Scheer for always being available for questions and discussions.

Lastly, I would like to thank my family, friends, and girlfriend Berna for their support and constant encouragement throughout my bachelor's studies.

Bibliography

[1] B. Lamic, J. S. Meyer, and M. Houzet, "Josephson radiation in a superconductor-quantum dot-superconductor junction," *Physical Review Research*, vol. 2, jul 2020.

[2] M. C. Cassidy, A. Bruno, S. Rubbert, M. Irfan, J. Kammhuber, R. N. Schouten, A. R. Akhmerov, and L. P. Kouwenhoven, "Demonstration of an ac josephson junction laser," *Science*, vol. 355, pp. 939–942, mar 2017.

[3] B. Josephson, "Possible new effects in superconductive tunnelling," *Physics Letters*, vol. 1, no. 7, pp. 251–253, 1962.

[4] R. P. Feynman, R. B. Leighton, and M. Sands, "The feynman lectures on physics: The definitive edition, volume iii," *Quantum Mechanics, Addison-Wesley*, 2006.

[5] D. E. McCumber, "Effect of ac Impedance on dc Voltage-Current Characteristics of Superconductor Weak-Link Junctions," *Journal of Applied Physics*, vol. 39, pp. 3113–3118, 11 2003.

[6] D. Scheer and F. Hassler, "On chip ac driving for dual shapiro steps," 2023.

[7] M. Tinkham, *Introduction to superconductivity*. Courier Corporation, 2004.

[8] P. Pietzonka, "Classical pendulum clocks break the thermodynamic uncertainty relation," *Physical Review Letters*, vol. 128, no. 13, p. 130606, 2022.

[9] C. Gerry and P. Knight, *Introductory Quantum Optics*. Cambridge University Press, 2005.

[10] L. Arndt, *Dual Shapiro steps of a phase-slip junction in the presence of a parasitic capacitance*. Master's thesis, 2018.

[11] J. Barry, E. Lee, and D. Messerschmitt, *Digital Communication*. No. Bd. 1, Springer US, 2004.

[12] A. Iserles, *Euler's method and beyond*, p. 3–18. Cambridge Texts in Applied Mathematics, Cambridge University Press, 2 ed., 2008.

[13] H. M. Moya-Cessa and F. Soto-Eguibar, *Differential equations: an operational approach*. Rinton Press, Incorporated, 2011.